Electronic Supplementary Material (ESI) for Physical Chemistry Chemical Physics.

More than protection: the function of TiO_2 interlayers in hematite functionalized Si Photoanode

Anurag Kawde [1,2,3,4], Alagappan Annamalai [5], Anita Sellstedt [6], Jens Uhlig[4], Thomas Wågberg[5], Pieter Glatzel [2], Johannes Messinger[1, 7*]*

[1] Umeå University, Faculty of Science and Technology Department of Chemistry, Sweden

[2] European Synchrotron Radiation Facility, Grenoble, France

[3]Lund Institute of advanced Neutron and X-Ray Science, Lund University, Sweden

[4] NanoLund and Chemical Physics, Department of Chemistry, Lund University, Sweden

[5] Umeå University, Faculty of Science and Technology, Department of Physics, Sweden

[6] Umeå University, Faculty of Science and Technology, Department of Plant Physiology, Umeå Plant Science Centre (UPSC), Umeå, Sweden

[7] Molecular Biomimetics, Department of Chemistry, Ångström Laboratory, Uppsala University, Sweden

[*] Corresponding authors- E-mail address: *pieter.glatzel@esrf.fr*

and

johannes.messinger@kemi.uu.se

EXPERIMENTAL METHODS

Synthesis and photo-electrochemical Characterization of functionalized n-Si photoelectrodes

n-Si MWs synthesis: A well-documented **m**etal-**a**ssisted electroless wet **c**hemical **e**tching (MACE) method was used to synthesis n-Si microwires (n-Si MWs) as described by Peng *et al.* .[1, 2] A n-type Si (100) with resistivity (1-10 ohm-cm) were purchased from Siegert Wafer- Germany. The n-Si wafer was sliced into 2×2 cm^2 pieces. These small n-Si pieces were ultrasonically cleaned in acetone, followed by isopropanol inside a fume hood. The n-Si pieces were then immersed in HF to etch any nascent oxide layer for 30-45 seconds and then immediately rinsed with water followed by drying in a dry nitrogen stream.

Two different electrolyte solutions were prepared for the synthesis of n-Si MWs. An electrolyte solution (E1) comprised of 4.6 M HF and 0.02 M $AgNO_3$. A second electrolyte solution (E2) comprised of 4.6 M HF and 0.02 M H_2O_2. HF was handled with recommended protective gear and under the fume hood. Cleaned n-Si pieces were first immersed in E1 for two minutes, to deposit Ag nanoparticles uniformly. These Ag nanoparticles coated n-Si pieces were then transferred into E2 and etched for 15 minutes. During MACE, a greenish-black silver dendritic debris is formed on top of n-Si MWs, which is removed by rinsing the silicon in water - HNO_3 solution (3:1 in volume).

TiO_2 sol-gel synthesis: The sol-gel coating procedure resulted in a mesoporous TiO_2 layer due to the well-known block co-polymer sol-gel assisted evaporation induced self-assembly (EISA) process[3, 4]. Here, the block-co-polymer Pluronic P123 acts as a templating agent, while titanium (IV) butoxide acts as the inorganic TiO_2 precursor. This led to spherical micelles, which upon aging and annealing resulted in the mesoporous structure. Figure SI 1 shows the SEM image of mesoporous TiO_2 (mp-TiO_2) coated on the planar n-Si substrate. For a more detailed

description, see for example [5].

The TiO_2 sol was prepared from Titanium (IV) butoxide, HCl (35.5%), Pluronic P123, and 1-butanol, in the molar ratio of 1:2:0.103:9. All chemicals were purchased from Sigma Aldrich-Sweden. First, the Titanium (IV) butoxide and HCl (35.5%) were mixed in a vial and magnetically stirred for 1 hour. Pluronic P123 and 2-butanol were mixed in a separate vial to be then combined with the Titanium mixture vigorously stirred for 24 hours. The TiO_2 sol obtained after 24 hours was then kept in the dark until further use.

TiO_2 coating on n-Si MWs: A spin-coating technique was employed to deposit a thin layer of TiO_2 onto n-Si MWs. Three cycles of 30 seconds each was programmed in a spin coater to rotate at 4000 rpm, and 1 ml of TiO_2 sol is dispensed on the n-Si MWs (2×2 cm^2). The TiO_2 coated n-Si MWs substrates were then kept on a platform equipped with a water bath inside a closed airtight chamber for 24 hours and under ambient conditions. The moisture exposed TiO_2 samples were annealed at 380^0 C in a nitrogen environment for two hours to yield the n-Si MWs/TiO_2 photoelectrode substrate.

Hematite deposition on n-Si MWs/TiO_2: The α-Fe_2O_3 nanorods on the n-Si MWs/TiO_2 structures were grown by the hydrothermal method as described by Vayssieres *et al.* .[6, 7] In brief, 0.15 M ferric chloride and 1 M sodium nitrate solutions were adjusted to pH 1.2 by dropwise addition of HCl. The n-Si MWs/TiO_2 substrates were soaked in this solution for 12 hours and kept under dry conditions in an autoclave at a constant temperature of 100°C. The n-Si MWs/TiO_2/α-Fe_2O_3 photoelectrodes were then rinsed with distilled water and ethanol followed by an annealing step at 380°C in a nitrogen environment for two hours.

Photo-electrochemistry: All the potential-current (linear sweep voltammetry-LSV) experiments were performed in an airtight photo-electrochemical cell equipped with a quartz

window. The chronoamperometric and photogenerated gas-evolution measurements were performed in a gas-tight three-electrode quartz cell from Pine Instruments, Durham-USA, equipped with an Ag/AgCl reference electrode and a platinum counter electrode. A solar simulator from Newport- 94043A, equipped with 450W Xenon lamp and air-mass 1.5 filter and a potentiostat from Metrohm Autolab (PGSTAT302N) was used to illuminate our photoelectrodes and perform the electrochemical measurements, respectively. All the photoelectrodes were illuminated at one sun condition with a power density of 100 mW/cm^2.

The linear sweep voltammetry was recorded at a scan rate of 20 mV/s with respect to an Ag/AgCl reference electrode and is reported in the main article as reversible hydrogen electrode potentials (V_{RHE}) using equation Eq. S1

$$V_{RHE} = V_{Ag/AgCl} + 0.1976 + (0.059 \times pH) \quad \text{Eq. S1}$$

The transient photocurrent responses for the functionalized n-Si MWs photoanodes were recorded in a two-electrode mode using an IviumStat-XRi potentiostat.

The photogenerated gases were measured by gas chromatography using a GC-8AIT gas chromatograph with a TCD detector (Schimadzu Scientific Instruments, Columbia, USA). 100 µl aliquots from the headspace of the photo-electrochemical cell were taken at regular intervals and analyzed in the GC-8AIT.

X-ray spectroscopy: The X-ray absorption and emission spectroscopy (XAS-XES) was carried out on beamline ID26 of the European Synchrotron radiation facility. A schematic view of the optics and the experimental set up is presented elsewhere.[8, 9] The high-energy resolution fluorescence detected X-ray absorption near edge structure (HERFD-XANES) and emission spectroscopies were performed at the Ti (K-α and β fluorescence line) and Fe K-β fluorescence line. A Si <311> double crystal monochromator was used to tune the incident beam at the Ti K-

edge. The incident X-ray energy was calibrated using Ti and Fe foils. The X-ray beam was focused on the sample and guarded by slits with size 0.7 mm in the horizontal and 0.2 mm in the vertical dimension. Higher harmonics were suppressed by total reflection using three Si mirrors at 2.5 mrad. The high-energy resolution fluorescence detected X-ray absorption near edge structure (HERFD-XANES) spectra were recorded at the maximum of the Ti and Fe $K\alpha_1$ line. The fluorescence energy was selected by two Ge (400), five Ge(331), and five Ge(620) for Ti Kβ, and Fe Kβ bent crystal analyzer (R=1m, r=100 mm), respectively, arranged in Rowland geometry.[8, 10] The X-ray photons selected by the crystal analyzers were focused onto an avalanche photodiode. The samples were placed into a fluorescence geometry, where the incident beam and the central crystal analyzer are at 45^0 with respect to the sample surface standard and at 90^0 angles between the incident beam and the central crystal analyzer. All HERFD-XANES and XES spectra reported here were normalized with respect to the total spectral area. Fluorescence-detected absorption spectra may show spectral distortions because of incident beam self-absorption or over-absorption effects.[11] One consequence of self-absorption may be an increased pre-edge spectral intensity. We did not correct the spectra for self-absorption but ensured that artefacts do not affect the conclusions drawn here.

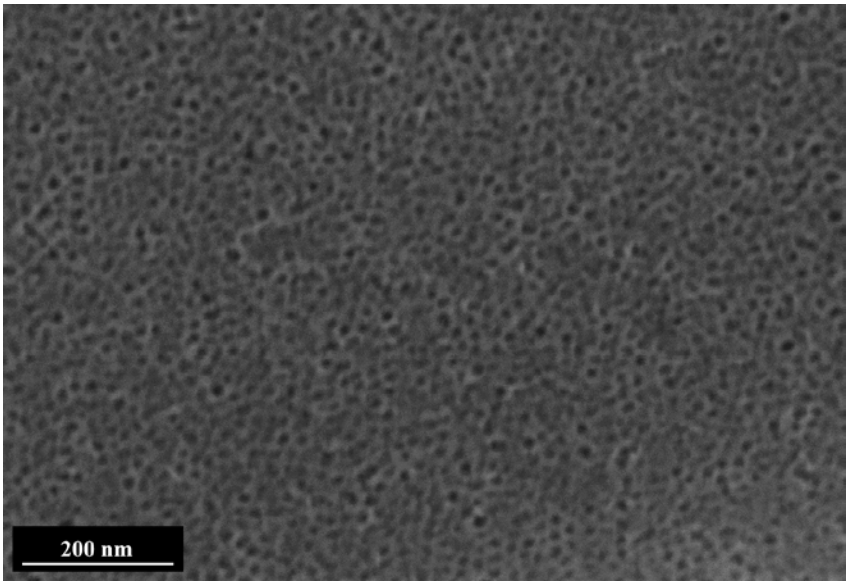

Figure SI 1: The SEM image showing the average pore size of mp-TiO_2 as 10 nm.

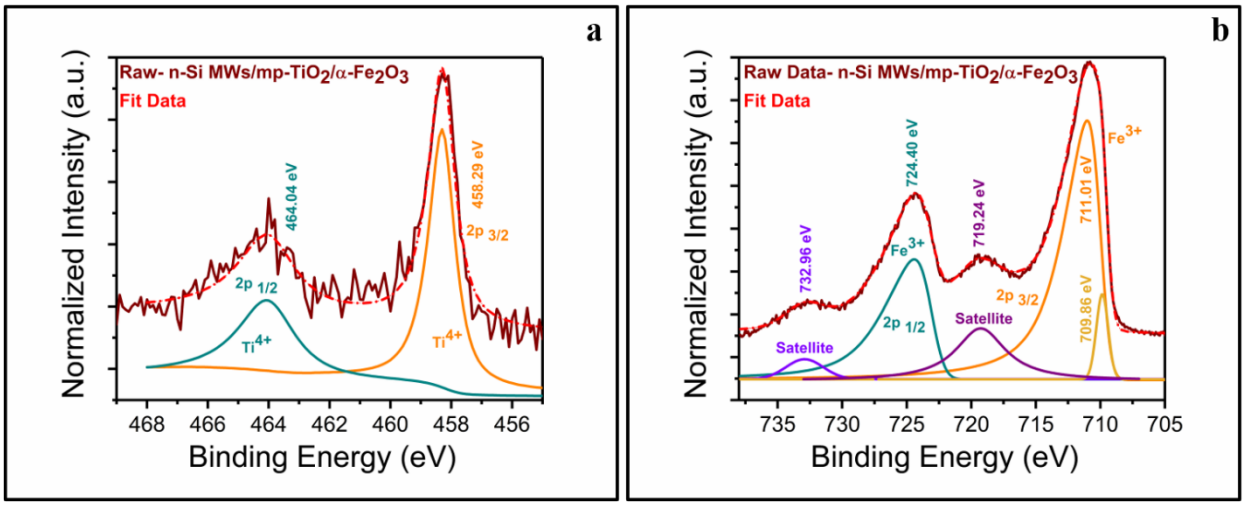

Figure SI 2: XPS spectra for **a)** n-Si MWs/mp-TiO_2/ α-Fe_2O_3 with $Ti2p_{3/2}$ (binding energy 458.29 ± 0.01 eV) and $Ti2p_{1/2}$ (binding energy 464.04 ± 0.01 eV) peaks confirming the Ti^{4+} surface species **c)** n-Si MWs/mp-TiO_2/ α-Fe_2O_3 with Fe $2p_{3/2}$ (binding energy 711.01 ± 0.01 eV) and Fe $2p_{1/2}$ (binding energy 724.40 ± 0.01 eV) peaks, indicating predominantly α-Fe_2O_3.

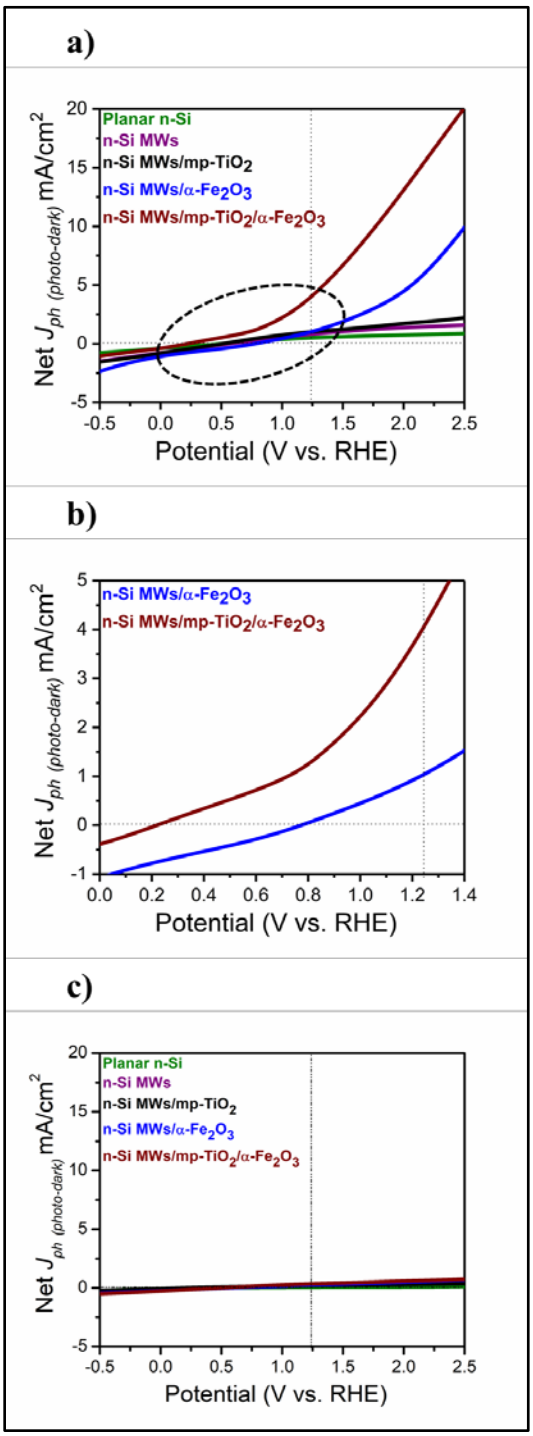

Figure SI 3: Linear sweep voltammograms recorded under 1 sun illumination in 1M NaOH (pH 13.9) **a)** planar n-Si, a surface etched n-Si with microwires (n-Si MWs), and functionalized n-Si photo-electrodes, **b)** magnified view of black dashed circle shown in **a)** comparing PEC performance of α-Fe_2O_3 nanorods grown on n-Si MWs with and without protective TiO_2 interlayer, and c) dark current.

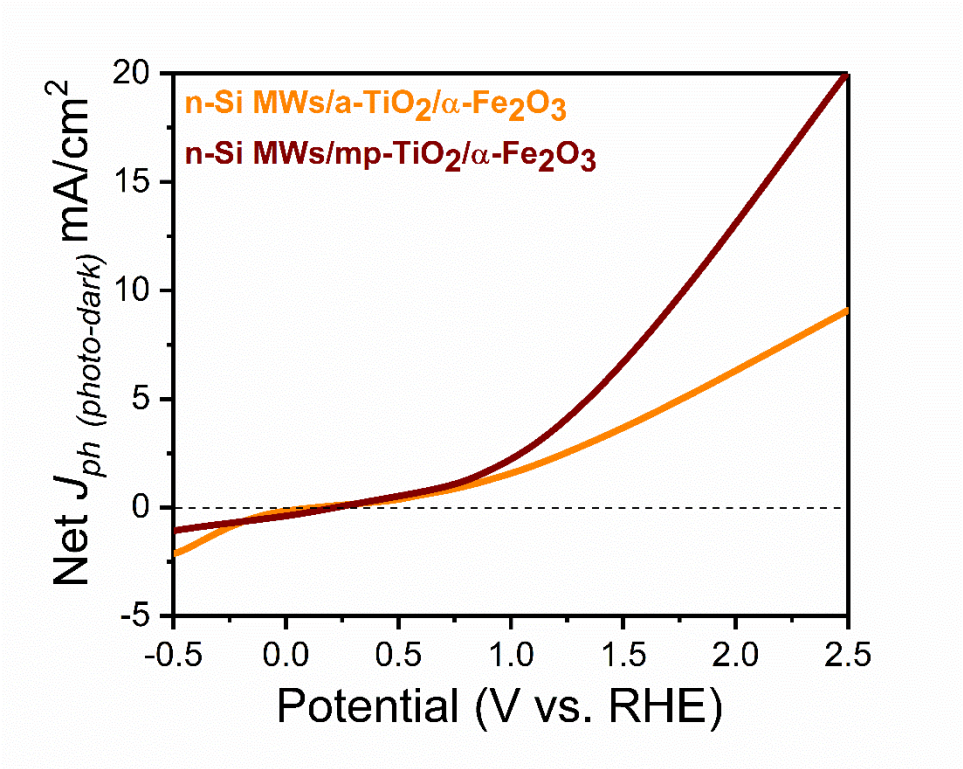

Figure SI 4: Linear sweep voltammograms showing significant increase in the J_{ph} on application of templated mesoporous TiO_2 protective layer (n-Si MWs/mp-TiO_2/ α-Fe_2O_3) compared to non-mesoporous amorphous TiO_2 layer (n-Si MWs/a-TiO_2/ α-Fe_2O_3).

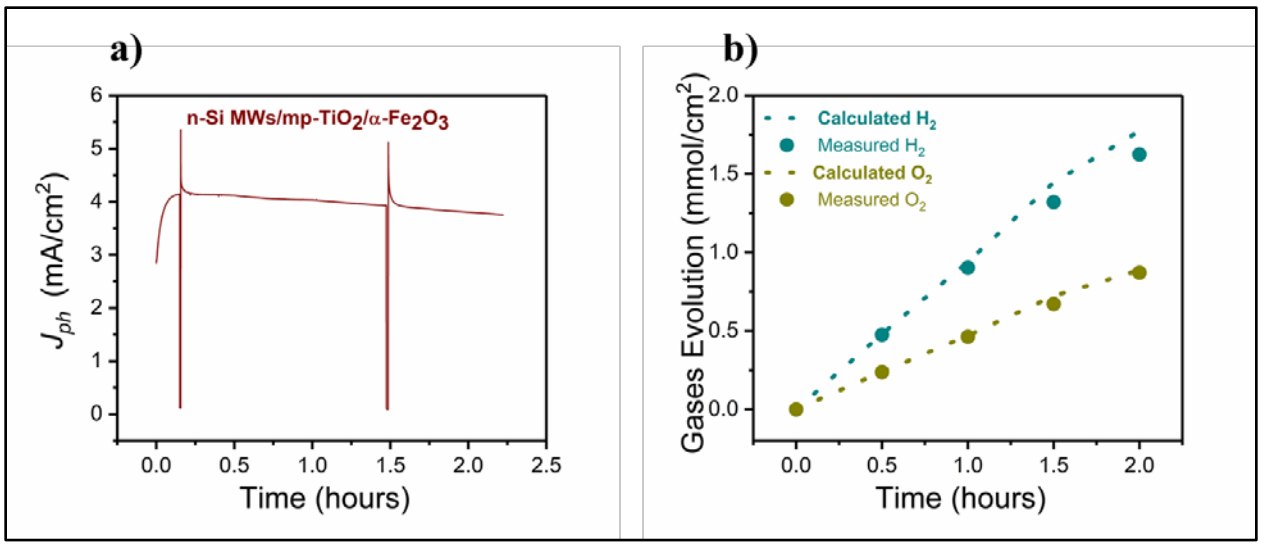

Figure SI 5: a) Chronoamperometry measurement performed at constant potential of 1.23 V_{RHE}, **b)** corresponding photogenerated gases were measured and analyzed using gas chromatography.

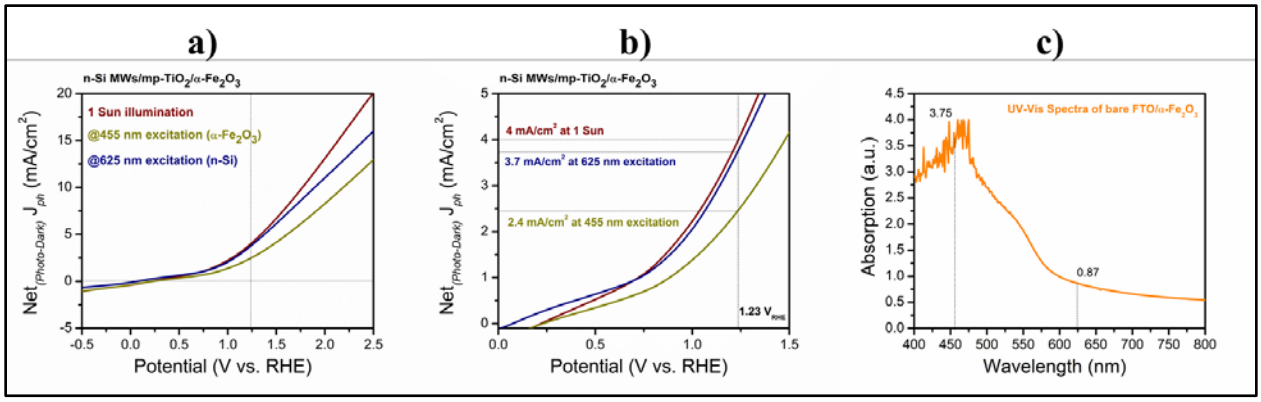

Figure SI 6: Linear sweep voltammograms a) and b) indicate that both n-Si MWs and α-Fe_2O_3 nanorods act as a dual absorber for n-Si MW/mp-TiO_2/α-Fe_2O_3 photoelectrode heterogeneous system, and UV-VIS absorption spectra of bare α-Fe_2O_3 nanorod.

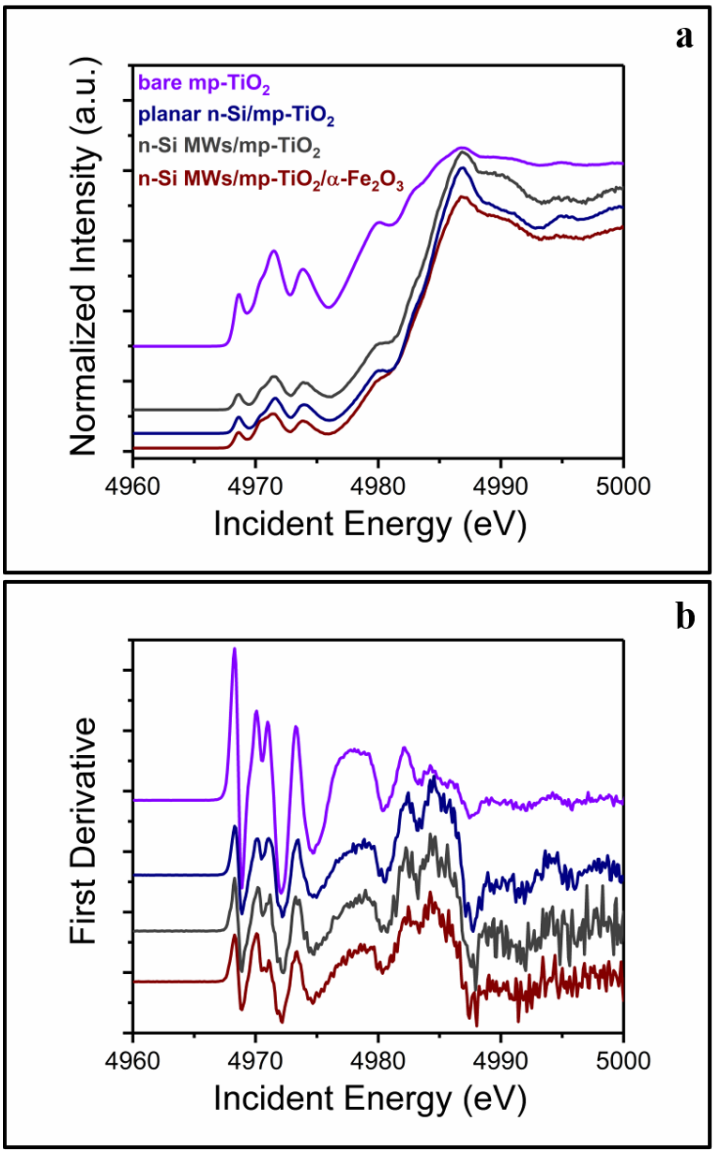

Figure SI 7: a) HERFD-XANES and **b)** first order derivative acquired at the Ti K-edge, for bare mp-TiO_2 as pellet, planar n-Si/mp-TiO_2, n-Si MWs/ mp-TiO_2 and n-Si MWs/ mp-TiO_2/α-Fe_2O_3.

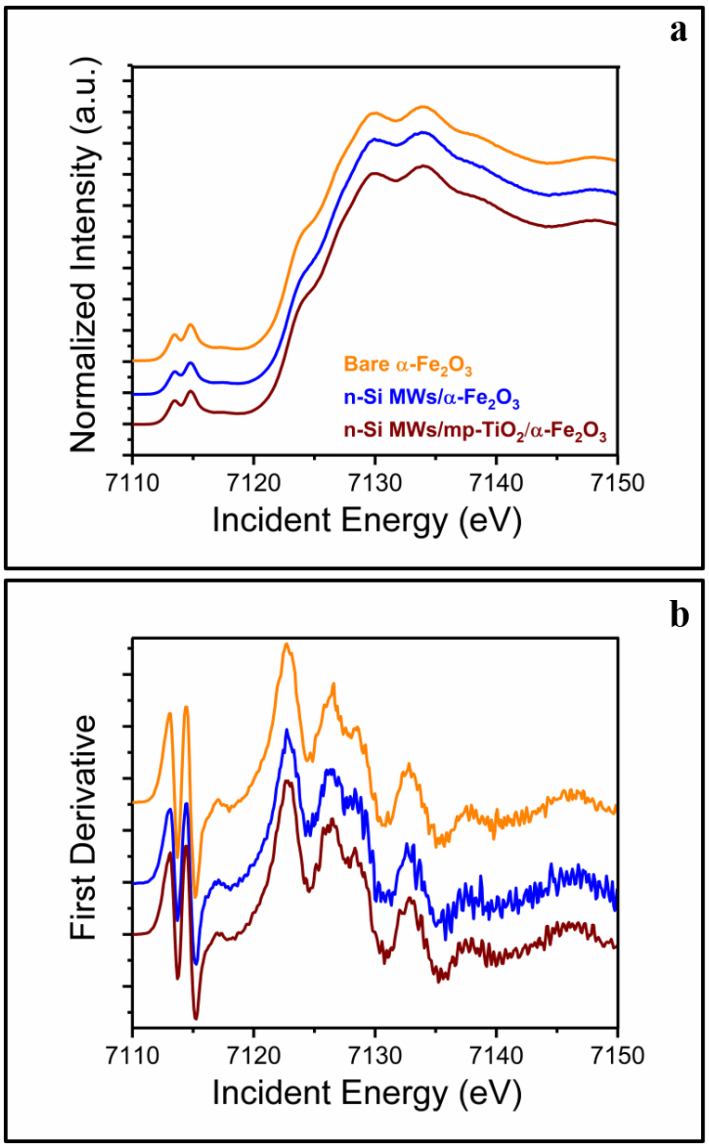

Figure SI 8: a) HERFD-XANES and **b)** first order derivative acquired at the Fe K-edge, for bare mp- α-Fe_2O_3 as pellet, n-Si MWs/ α-Fe_2O_3 and n-Si MWs/ mp-TiO_2/α-Fe_2O_3.

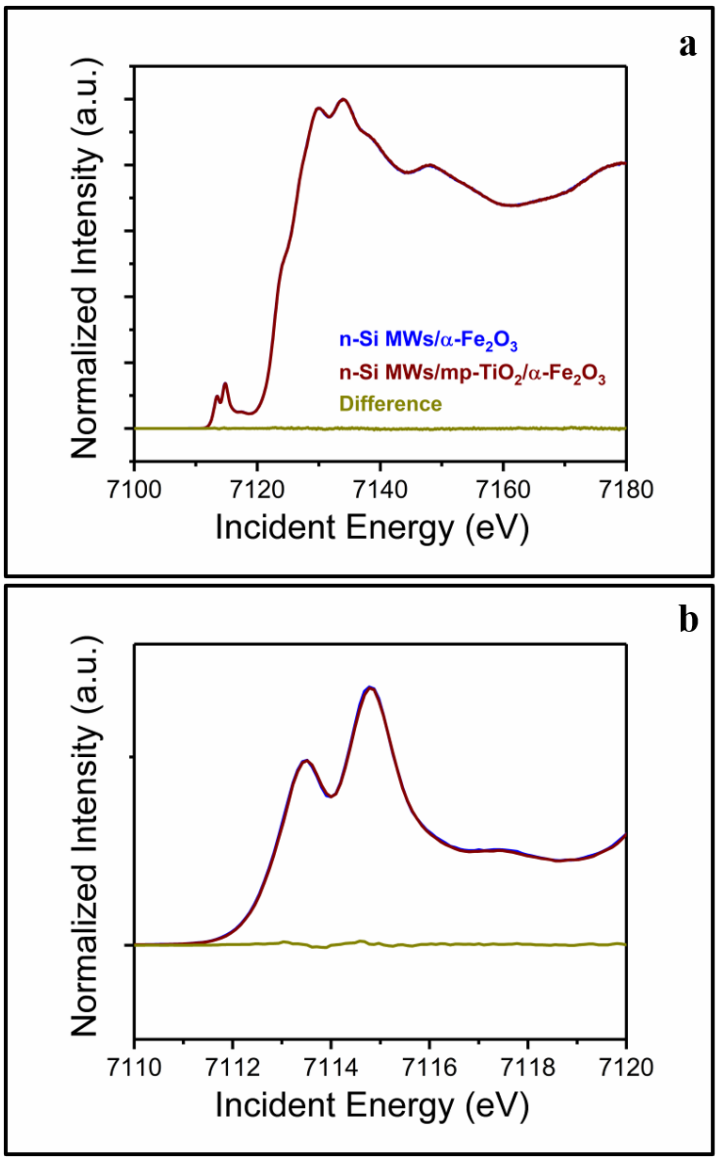

Figure SI 9: HERFD-XANES acquired at the Fe K-edge comparing n-Si MWs/ α-Fe_2O_3 and n-Si MWs/ mp-TiO_2/α-Fe_2O_3. The difference spectrum shows that presence of mp-TiO_2 interlayer do not induce any significant electronic changes in the α-Fe_2O_3.

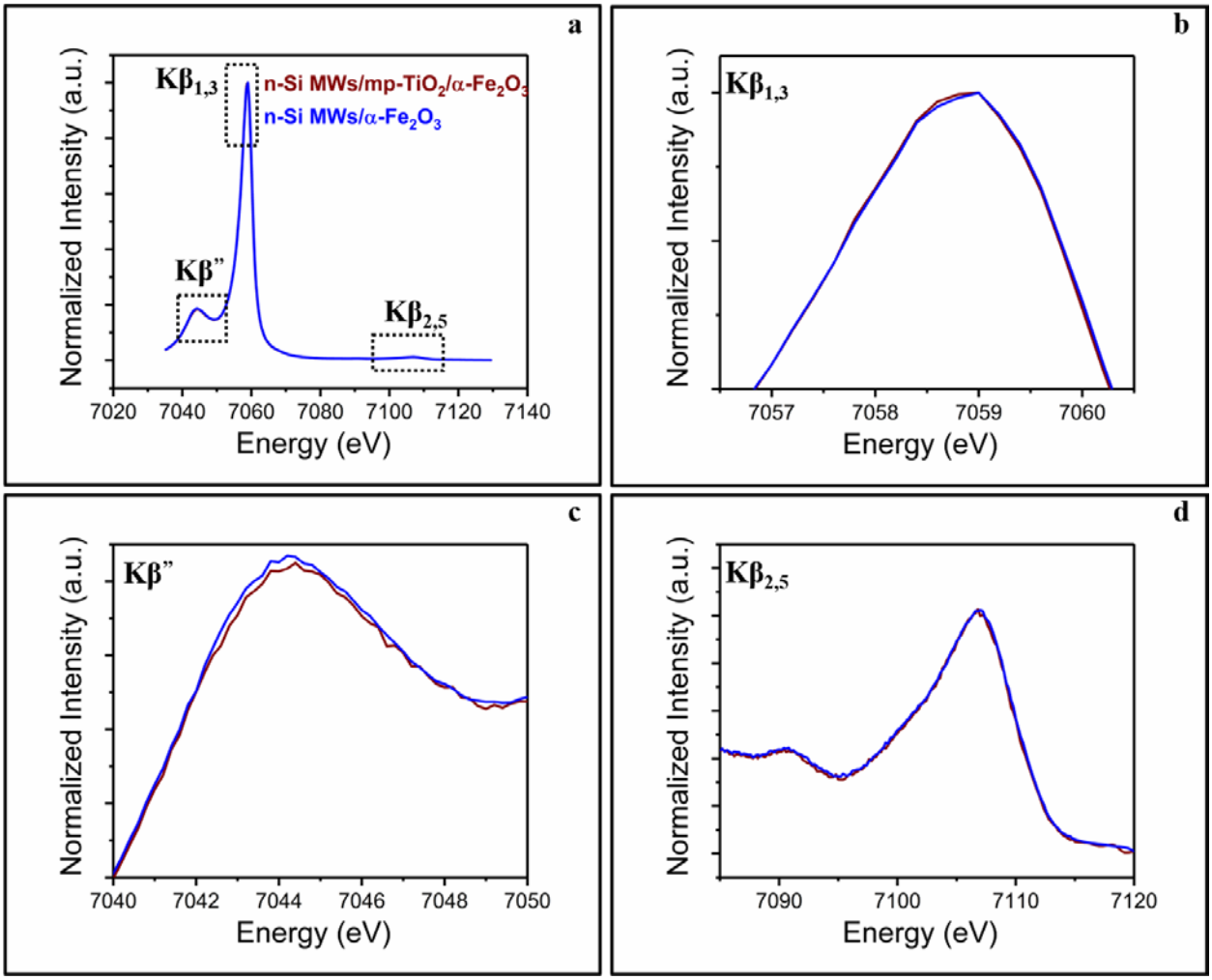

Figure SI 10: Fe Kβ XES spectra acquired for functionalized n-Si MWs photoanodes with **a)** Kβ main and vtc-XES, **b)** $K\beta_{1,3}$, **c)** Kβ' and **d)** $K\beta_{2,5}$.

Approximate estimation of the interfacial contact volume of mp-TiO_2 and α-Fe_2O_3

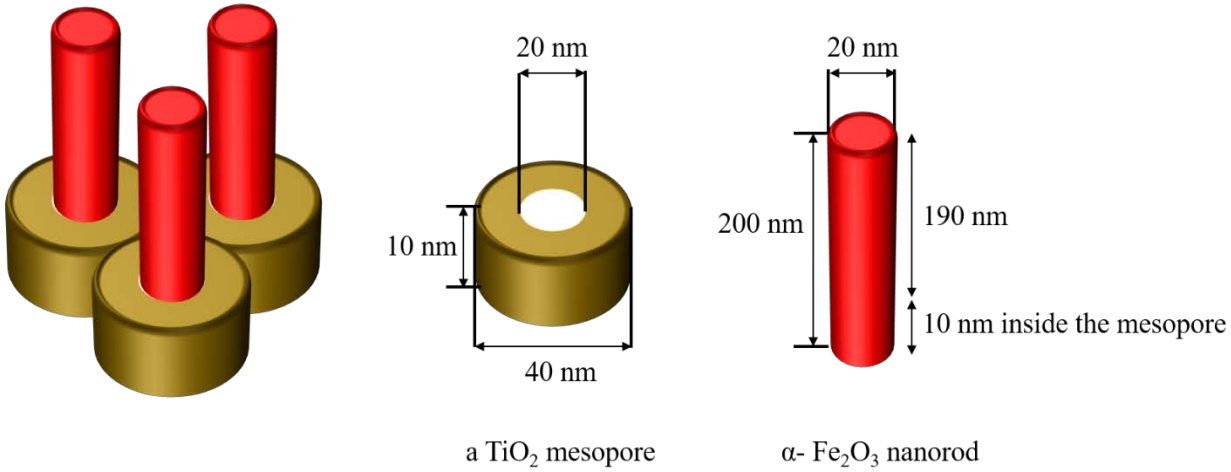

Figure SI 11: Schematic representation for the dimensions and interaction of mp-TiO_2 with α-Fe_2O_3 nanorods.

The dimensions of the α-Fe_2O_3 nanorods are estimated from the SEM image shown in Figure 1.

The dimensions of mp-TiO_2 are estimated form the SEM image reported in our previous study[5, 12]

and in the Figure SI 1.

Fraction of α-Fe_2O_3 in contact with mp-TiO_2

Approximate diameter of α-Fe_2O_3 nanorod: 20 nm

Approximate depth of a TiO_2 mesopore :10 nm

Approximate length of hematite nanorod inside a mesopore of TiO_2: 10 nm

Thus, approximately volume of one α-Fe_2O_3 nanorod inside a mesopore TiO_2 is

Case 1: considering whole of α-Fe_2O_3 nanorod (20 nm diameter, and 10 nm inside mesopore) in contact with mp-TiO_2 inside a mesopore

$(V = \pi r^2 h)$ (3.14 × 10^2 × 10) = ~ 3142 nm^3

Total approximate volume of one α-Fe_2O_3 nanorod for approximate length of 200 nm is

($V = \pi r^2 h$) (3.14× 10^2 × 200)= 62831 nm^3

Fraction of α-Fe_2O_3 in contact with TiO_2 is (3142/62831) × 100 = ~ 4.6 %

Case 2: considering part of α-Fe_2O_3 nanorod in contact with mp-TiO_2 inside a mesopore

(V=πr^2 h) [3.14 × (5^2) × 10)] = ~ 785 nm^3 (minimum)

Fraction of α-Fe_2O_3 in contact with TiO_2 is (785/62831) × 100 = ~ 1.2 % (minimum)

Fraction of mp-TiO_2 in contact with α-Fe_2O_3

Approximate diameter of one mesopore of TiO_2: 20nm

Approximate wall thickness of a mesopore of TiO_2: 10 nm

Approximate depth of a TiO_2 mesopore :10 nm

Approximate volume of TiO_2 around one pore:

Case 1: considering complete mesopore of TiO_2 is in contact with the α-Fe_2O_3 nanorod

(volume of outer pore -volume of inner pore) = (12567-3141)= 9426 nm^3 (maximum)

Based on our previous study, the approximate thickness of TiO_2 around a Si MWs is 50nm, therefore total TiO_2 content considering 10 nm pores over 50 nm thick TiO_2 : 9426*5 = 47130 nm^3

Fraction of TiO_2 in contact with α-Fe_2O_3 is (9426/47130) × 100 = 20 %

Case 2: considering part of mesopore of TiO_2 in contact with the α-Fe_2O_3 nanorod

(V=πr^2 h) [3.14 × (15^2 – 10^2)× 10] = ~ 3927 nm^3

Fraction of TiO_2 in contact with α-Fe_2O_3 is (3927/47130) × 100 = 8.33 %

Experimental estimation of interfacial contact of mp-TiO_2 and α-Fe_2O_3

The pre-edge region for n-Si MWs/ mp-TiO_2/α-Fe_2O_3 and n-Si MWs/ mp-TiO_2, along with the difference spectra, is shown in Figure SI 12 a. The deconvoluted spectra for n-Si MWs/ mp-TiO_2/α-Fe_2O_3, n-Si MWs/ mp-TiO_2, and difference spectra are shown in Figure SI 12 b-d, respectively. As the electronic structural change at TiO_2 pre-edge is mainly observed at the pre-edge peak A2 and A2*, experimental estimation of interfacial contact between mp-TiO_2 and α-Fe_2O_3 was assessed by taking the percentage of area in fit peak 2 of Figure SI 12 d (difference spectra) by cumulative area of fit peak 2 and 3 of Figure SI 12 b and c. The area obtained for each peak after deconvolution is given in Table 1.

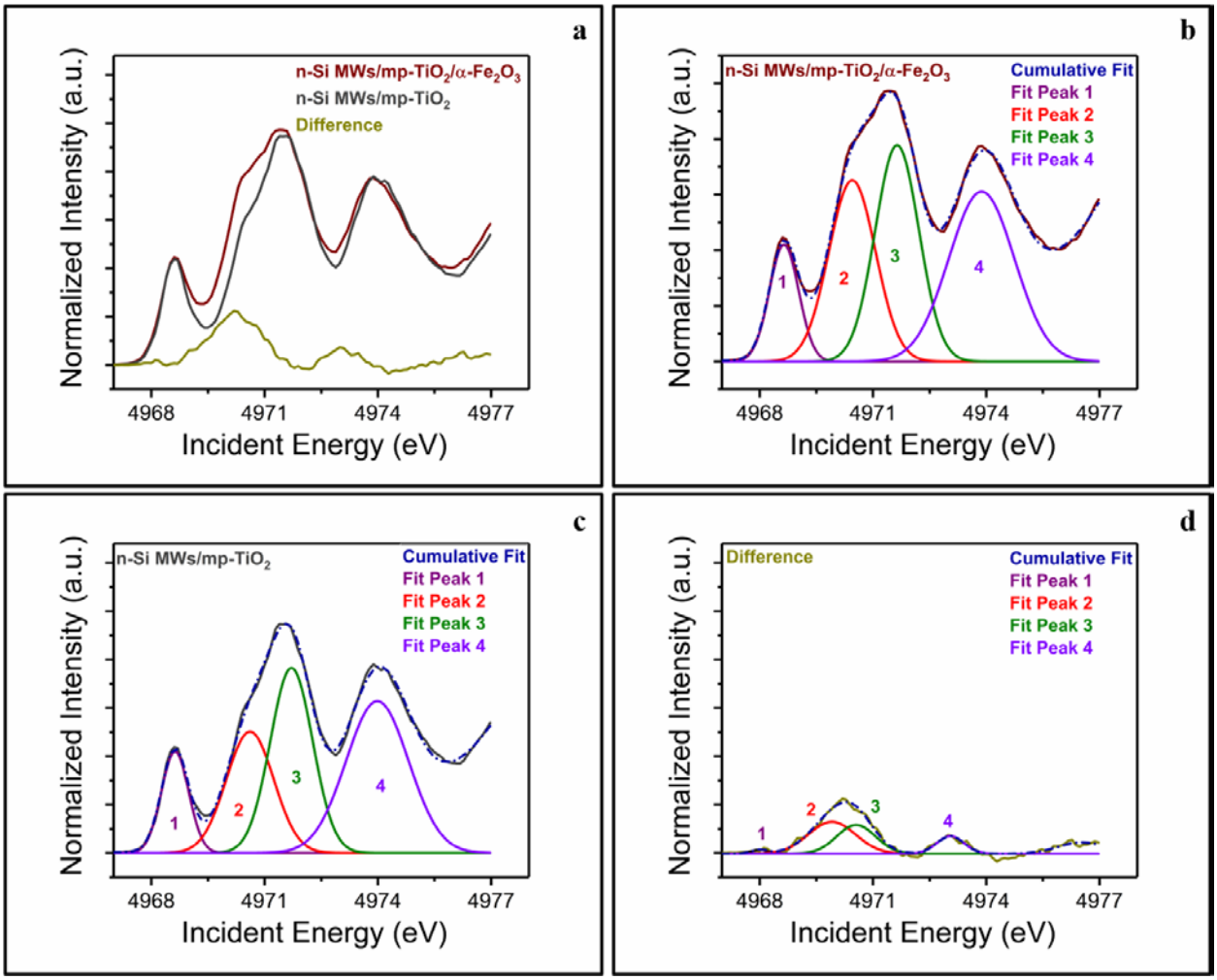

Figure SI 12: a) Pre-edge HERFD-XANES spectra acquired for functionalized n-Si MWs photoanodes at the Ti K-edge and deconvoluted spectral peaks for **b)** n-Si MWs/ mp-TiO_2/α-Fe_2O_3 **c)** n-Si MWs/ mp-TiO_2 and **d)** difference.

	n-Si MWs/ mp-TiO_2/α-Fe_2O_3	**n-Si MWs/ mp-TiO_2**	**Difference**	**% Change**
Peak 1	$0.001 \pm 2.6E^{-5}$	$9.5E^{-4} \pm 2.7E^{-5}$	$2.28\ E^{-5} \pm 9.7E^{-6}$	1.16
Peak 2	$0.0026 \pm 2.2E^{-4}$	$0.002 \pm 3.2E^{-4}$	$5.16\ E^{-4} \pm 0.002$	11.21
Peak 3	$0.0029 \pm 2.28E^{-4}$	$0.0027 \pm 3.2E^{-4}$	$3.82\ E^{-4} \pm 0.002$	6.82
Peak 4	$0.003 \pm 1.2E^{-4}$	$0.0033 \pm 1.4E^{-4}$	$1.65\ E^{-4} \pm 1.03\ E^{-5}$	2.61
Average	$2.38\ E^{-3}$	$2.23\ E^{-3}$	$2.71\ E^{-4}$	5.45

Table 1: Peak area obtained for the deconvoluted peaks shown in Figure SI 12

For example:

The percentage change in the difference spectra considering the area under peaks 2 and 3 can be computed as,

$$\frac{Area\ of\ Peak2\ (difference\ spectra)}{Cumulative\ area\ of\ peak\ 2\ and\ 3\ (\text{functionalized Si MWs})} \times 100$$

$$= [((5.16 + 3.82) \times 10^{-4})/(0.0026 + 0.0029 + 0.002 + 0.0027)] \times 100$$

$$= 8.80\ \%$$

References:

1. K. Peng, Y. Wu, H. Fang, X. Zhong, Y. Xu and J. Zhu, *Angew. Chem., Int. Ed.*, 2005, **44**, 2737-2742.
2. K. Peng, Y. Xu, Y. Wu, Y. Yan, S. T. Lee and J. Zhu, *Small*, 2005, **1**, 1062-1067.
3. K. Liu, H. Fu, K. Shi, F. Xiao, L. Jing and B. Xin, *J. Phy. Chem. B*, 2005, **109**, 18719-18722.
4. S. Y. Choi, M. Mamak, N. Coombs, N. Chopra and G. A. Ozin, *Adv. Fun. Mat*, 2004, **14**, 335-344.
5. A. Kawde, A. Annamalai, L. Amidani, M. Boniolo, W. L. Kwong, A. Sellstedt, P. Glatzel, T. Wågberg and J. Messinger, *Sus. Energy and Fuels*, 2018, **2**, 2215-2223.
6. L. Vayssieres, N. Beermann, S.-E. Lindquist and A. Hagfeldt, *Chem. Mater.*, 2001, **13**, 233-235.
7. A. Annamalai, P. S. Shinde, A. Subramanian, J. Y. Kim, J. H. Kim, S. H. Choi, J. S. Lee and J. S. Jang, *J. Mater. Chem. A*, 2015, **3**, 5007-5013.
8. M. Rovezzi and P. Glatzel, *Semi. Sci. Tech.*, 2014, **29**, 023002.
9. L. Amidani, A. Naldoni, M. Malvestuto, M. Marelli, P. Glatzel, V. Dal Santo and F. Boscherini, *Angew. Chem., Int. Ed.*, 2015, **54**, 5413-5416.
10. P. Glatzel and U. Bergmann, *Co. Chem. Rev.*, 2005, **249**, 65-95.
11. M. Bianchini and P. Glatzel, *J. Sync. Rad.*, 2012, **19**, 911-919.
12. A. Kawde, A. Annamalai, A. Sellstedt, P. Glatzel, T. Wågberg and J. Messinger, *Dalton Transc.*, 2019, **48**, 1166-1170.